Long-Term Stability and High Flux Membrane Prepared Through Intramembrane Dopamine-Based Nanoparticle Assembly

Yu Ma[a] *‡, Fang Gao[a,b]‡, Rui Pan[a], Zhongyi Jiang[c], Xiaoli Zhao[d], Yi Wang[b], Bin He[a] *

[a] Institute of Eco-Environmental and Soil Sciences, Guangdong Academy of Sciences, Guangzhou 510650, China.

[b] School of Environmental Science and Engineering, Guangdong University of Technology, Guangzhou 510006, China.

[c] Key Laboratory for Green Chemical Technology of Ministry of Education, School of Chemical Engineering and Technology, Tianjin University, Tianjin, 300072, China.

[d] State Key Laboratory of Environmental Criteria and Risk Assessment, Chinese Research Academy of Environmental Sciences, Beijing 100012, China.

* Corresponding author. Email: bhe@soil.gd.cn, yma@soil.gd.cn

‡ Y. Ma and F. Gao contributed equally to this work.

Abstract

Stable geometric chemical structures can ensure the long-term stability of separation membranes for water treatment. In this study, polydopamine (PDA)/polyethyleneimine (PEI) nanoparticle (PDA/PEI-NP) membranes are prepared using a vacuum-assisted self-assembly technique, in which PDA/PEI NPs are supported inside the polymer membrane. During the self-assembly process, highly adhesive NPs, which exhibit the formation of bonds, are selectively supported at the dead end of the membrane pores. This phenomenon inhibits the leaching caused by the fluid-induced erosion of traditional coatings. Therefore, the obtained membranes exhibit excellent long-term stability. Additionally, the membrane flux increases after modification because the NPs do not block the flow-through pores and the abundant hydrophilic groups decrease the threshold pressure across the membrane. The pure water permeability of the proposed membrane is 10,647± 49 $L \cdot m^{-2} \cdot h^{-1} \cdot bar^{-1}$, which is 11.52% higher than that of the PDA/PEI co-deposited blank membranes. The proposed facile approach to develop stable and high-performance membranes is expected to facilitate the sustainable development of membrane technologies.

Keywords: polydopamine/polyethyleneimine nanoparticles, intramembrane nanoparticle assembly, selective support, long-term stability, high flux

1. Introduction

Water shortage and water quality deterioration are challenges that are being frequently encountered in the 21st century [1]. As a promising water treatment technology with a low energy consumption, membrane separation technologies are being widely incorporated [2]. To enhance the advantages of using such technologies, separation membranes that can exhibit long-term stability and excellent separation performance must fabricated using facile approaches [1–5]. A representative method for preparing high-performance membranes is to coat a functional layer on (or inside) the membranes [6]. However, these coatings are typically unstable owing to the absence of strong interactions between the coating and membrane surface, resulting in inferior long-term stability and limited applications [6–8].

To solve these problems, interface regulation has been used to enhance interactions through the formation of chemical bonds [5]. Polydopamine (PDA) coatings, which are simple and effective materials, are desirable candidates for this regulation [9], PDA contains amino, phenolic hydroxyl, benzene ring, catechol, indoles, and quinoid groups, which can interact and react with many materials through hydrogen bonding, π–π bonds, metal–ligand interactions, Michael addition, and Schiff base reactions [10]. Consequently, membranes with PDA coatings exhibit stable performance [11–15].

To achieve highly efficient separation, hydrophilic groups have been introduced to fabricate hydrophilic and underwater superhydrophobic membranes [16]. By introducing a hydration layer with high viscosity and low solubility onto the hydrophilic membrane surface to develop physical and energy barriers against foulants, the foulants could be adsorbed and antifouling performance could be achieved [17,18]. Various studies have indicated that the hydrophilicity can be enhanced to increase the membrane flux [19]. In particular, water treatment membranes have an intrinsic threshold pressure, and their permeability can only be stabilized when the pressure difference across the membrane exceeds this pressure. Enhancing the hydrophilicity of a membrane can help decrease the threshold pressure. In this scenario, the membrane can be wetted by water at a lower pressure, thereby increasing the membrane flux [20,21].

Considering these aspects, researchers focused on dopamine-based modified membranes to achieve long-term stable performance and a high separation efficiency. Based on PDA/polyethyleneimine (PEI) co-deposition, Xu et al. designed a membrane that is superhydrophilic in air and superhydrophobic in water. The maximum water permeability was approximately 7000 $L \cdot m^{-2} \cdot h^{-1} \cdot bar^{-1}$, and the membrane exhibited high stability in acidic, neutral, and weakly alkaline solutions [15]. Shao et al. filtered a mixed solution of trimethoxysilylpropyl octadecyldimethyl ammonium chloride-dopamine-Tris-HCl into the interior of a poly(1,1-difluoroethylene) (PVDF) membrane. Through further polymerization, a polydopamine-modified membrane with excellent antipollution performance was obtained [22].

In this study, a membrane with long-term stability and excellent separation performance was fabricated using a facile approach. PDA/PEI-nanoparticle (NP) membranes were prepared through the vacuum filtration of a PDA/PEI-NP dispersion to support NPs in the interior of the PDA/PEI-co-deposited PVDF membrane (**Scheme 1**). First, the highly adhesive NPs were smaller than the membrane pores, and the pores were tortuous. Therefore, the NPs did not remain in the flow-through pores during filtration. Instead, the NPs selectively accumulated at the dead end of the pores, which inhibited NP leaching and produced a new pore wall. Second, in contrast to the reversible coordination bonds between the co-deposition layer and hydrophobic materials, covalent bonds were formed in the NPs via Michael addition or the Schiff base reaction [9,10,15,23,24], which inhibited the leaching of polymers on the NP surface owing to creeping flow inside the membrane. Therefore, the obtained membranes were expected to exhibit excellent long-term stability. Moreover, because the NPs did not block the flow-through pores and contained abundant hydrophilic groups, the membrane flux increased, and the antifouling performance was enhanced. This study represents the first attempt at selectively supporting NPs inside a polymer membrane to realize long-term stability and excellent separation performance using a facile method. The findings are expected to guide the sustainable development of membrane technologies.

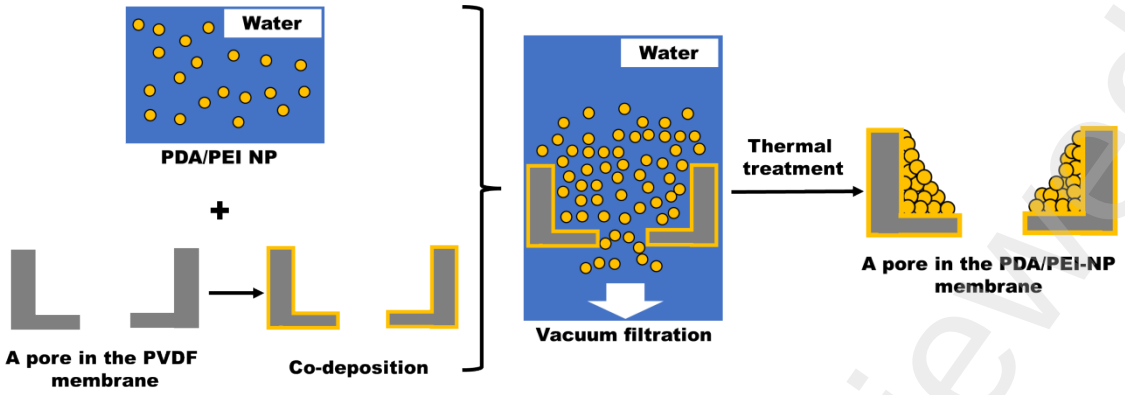

Scheme 1. Preparation of the PDA/PEI-NP membrane.

2. Results and Discussion

2.1 Morphology and chemical composition of the PDA/PEI NPs

The morphology of the PDA/PEI NPs was characterized through field emission scanning electron microscopy (FESEM). As shown in **Figure 1a**, most PDA/PEI NPs exhibited a spherical structure and uniform particle size. Quantitative characterization using a laser particle size analyzer (Figure 1b) indicated that the size distribution of the NPs was concentrated in the range of 164–225 nm, with an average particle size of 217 nm. When PDA/PEI NPs were dispersed in water, a significant Tyndall effect was observed upon laser illumination (Figure 1c), indicating that the NPs exhibited colloidal properties and could develop a highly dispersed heterogeneous system in water.

The chemical structures of the PDA/PEI NPs were analyzed through Fourier transform infrared spectroscopy (FTIR) and X-ray photoelectron spectroscopy (XPS) analyses. The FTIR spectrum of dopamine (Figure 1d) indicated that the absorption peaks of PDA were mainly located at 1617 cm^{-1}, 1519 cm^{-1}, and 1289 cm^{-1}, which corresponded to C=C bonds, bending vibration of N-H bonds, and stretching vibrations of C-N bonds in aromatic rings, respectively. In accordance, the absorption peaks of the PDA/PEI NPs appeared at 1633 cm^{-1} and 1365 cm^{-1}. The absorption peak at 1365 cm^{-1} corresponded to C-N bonds, which reflected the presence of PEI fragments in the NPs. PEI reacted with PDA through the Michael addition reaction (in general, the C-N bond is sensitive to chemical environments, and its presence in PEI leads to a red-shift of the corresponding absorption peak). Additionally, the absorption peak at 1633 cm^{-1} was broader than that of PDA owing to the formation of a C=N bond between PDA and PEI, indicating the reaction of PDA with PEI. Figure 1e presents the chemical composition of the

PDA/PEI NPs, characterized by XPS. The NPs mainly contained C, N, and O. The N 1*s* high-resolution narrow spectrum shown in Figure 1f confirmed the formation of a C=N bond between PDA and PEI through a Schiff base reaction.

These results indicated that the NPs had a regular shape, narrow size distribution, and highly uniform dispersion. Notably, C-N and C = N covalent bonds were formed in the NPs through the Michael addition and Schiff base reactions between PDA and PEI.

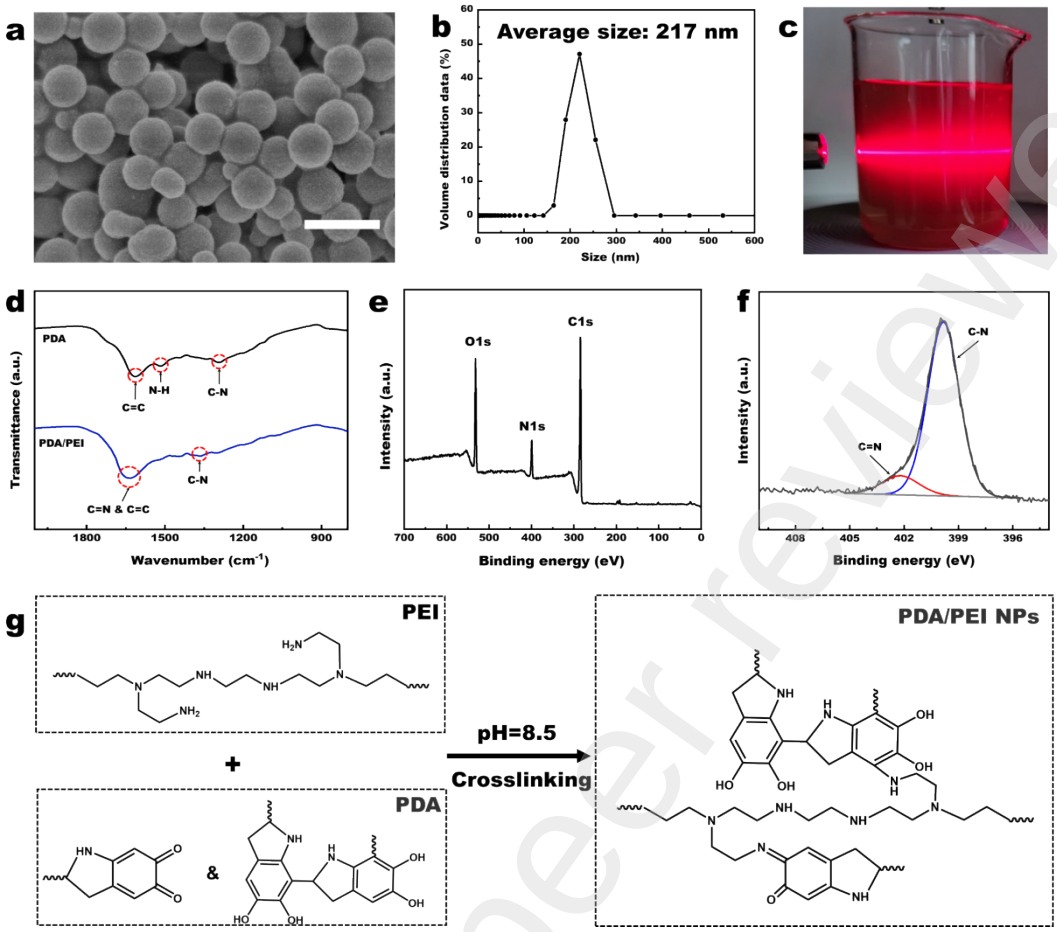

Figure 1. Morphology and chemical composition of the PDA/PEI NPs. (a) Morphology (scale bar = 500 nm); (b) Size distribution; (c) Tyndall effect of PDA/PEI-NP dispersion; (d) FTIR spectra of PDA and PDA/PEI NPs; (e) Broad-scan XPS spectrum of PDA/PEI NPs; (f) Narrow-scan XPS N 1*s* spectrum of PDA/PEI NPs; (g) Schematic of the possible chemical reaction between PDA and PEI.

2.2 Geometrical–chemical structure of the NP membranes

In this study, PDA/PEI-NP membranes were prepared by supporting PDA/PEI NPs on a co-deposited PVDF membrane. The surface and cross-sectional morphologies of the PVDF, co-deposited, and PDA/PEI-NP membranes were characterized by FESEM (**Figure 2a–f**). As shown in Figure 2a and 2d, the PVDF membrane exhibited a porous structure with tortuous channels. The surface and cross-sectional morphologies of the PDA/PEI co-deposition-modified membrane were similar to those of the PVDF membrane (Figure 2b and 3e), indicating uniform deposition of PDA/PEI on the surface of the PVDF membrane. When NPs were supported on the co-deposited membrane through vacuum-assisted filtration, they were observed in the membrane pores and did not block the flow-through pores (Figure 2c and 2f).

The chemical structures of the PVDF, co-deposited, and PDA/PEI-NP membranes were analyzed through attenuated total reflection (ATR)/FTIR and XPS (Figure 2g–h). In contrast to the PVDF membrane, absorption peaks appeared at 1655 cm^{-1} and 1645 cm^{-1} in the spectra of the co-deposited and PDA/PEI-NP membranes (Figure 2g), which indicated the stretching vibration of C=N and C=C bonds in the aromatic rings, respectively. This observation confirmed that PDA and PEI reacted with each other in the co-deposited and PDA/PEI-NP membranes. According to the wide-scan XPS spectra (Figure 2h), N and O were observed on the surfaces of the co-deposited and PDA/PEI-NP membranes, indicating the presence of PDA/PEI. The contents of O, N, and C on the surface of the co-deposited and PDA/PEI-NP membranes were 8.07%, 7.67%, and 58.92% and 14.35%, 11.69%, and 61.69%, respectively. In other words, the O/C and N/C ratios increased from 13.70% and 13.02% to 23.26% and 18.95%, respectively, after support, suggestive of the increased densities of O and N on the surface of the PDA/PEI-NP membrane after support.

These results indicated that the PDA/PEI NPs were supported inside the membrane through vacuum-assisted filtration. Because the pore diameter was larger than that of the NPs and the NP concentration was low, the NPs could not block the flow-through pores during vacuum filtration. Moreover, owing to the tortuous channels in the polymer membrane, the NPs could be supported at the dead end around the flow-through pores, forming a new pore wall (Scheme 1 and Figure 2f). Consequently, the NPs were less susceptible to being washed away by the fluids. The O and N densities on the NP membrane surface were 1.77 and 1.46 times higher than those of the co-deposited membrane, respectively, indicating that the supporting of NPs

increased the content of hydrophilic groups such as hydroxyls and imines on the membrane surface. The overall hydrophilicity of the membrane was enhanced because the NPs were mainly supported inside the membrane. Finally, the membrane color intensified after the NP support (Figure 2i), providing visual evidence of the successful preparation of the PDA/PEI-NP membrane.

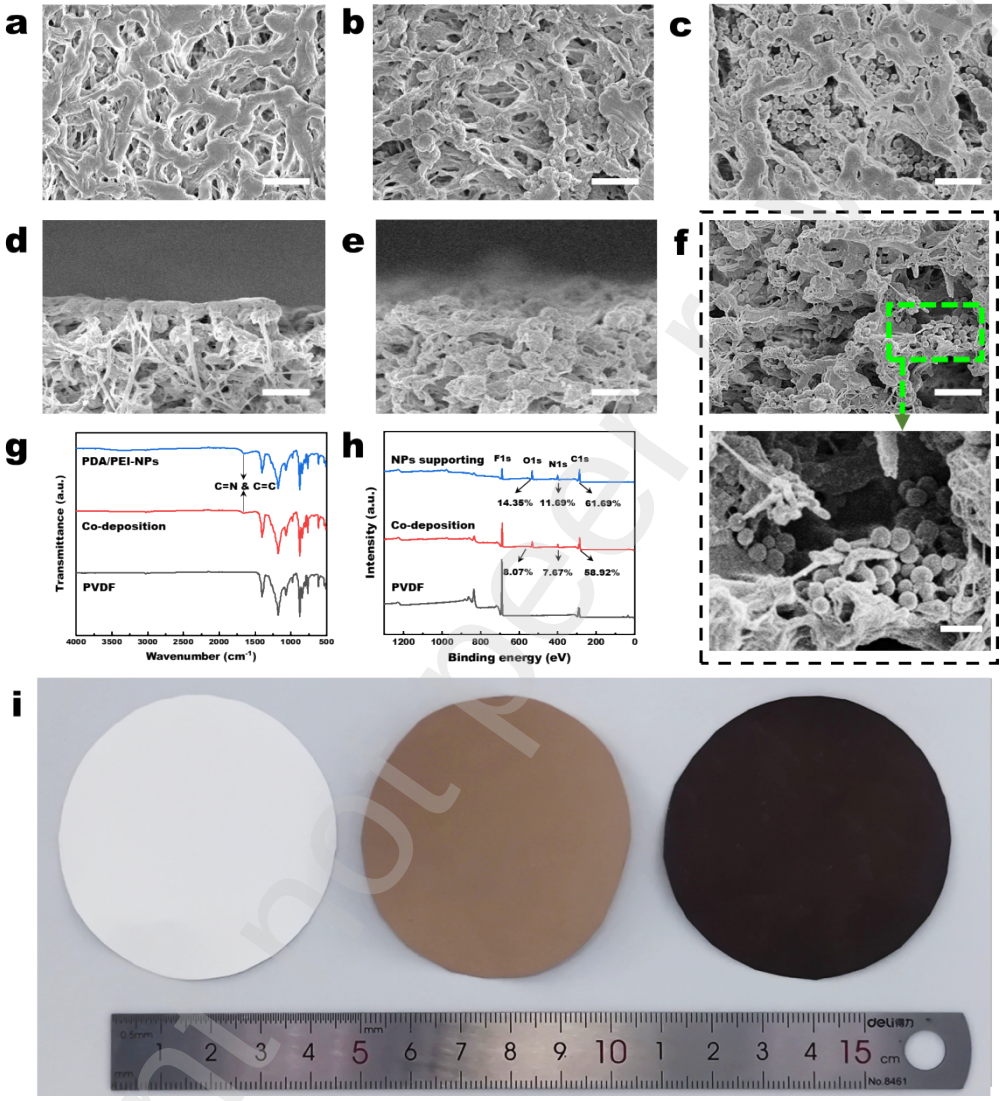

Figure 2. Morphology and chemical composition of the membranes. (a) Surface and (d) cross-sectional morphologies of the PVDF membrane (scale bar = 2 μm). (b) Surface and (e) cross-sectional morphologies of the co-deposited membrane (scale bar = 2 μm). (c) Surface and (f) cross-sectional morphologies of the PDA/PEI-NP membrane (scale bar = 2 μm, 2 μm, and 500 nm in c, f (upper) and f (lower), respectively). (g) FTIR/ATR spectra and (h) XPS spectra of the PVDF, co-deposited, and PDA/PEI-NP membranes. (i) Images of the PVDF membrane (left), co-deposited membrane (middle), and NP membrane (right).

2.3 Stability of NPs in membranes

The stability of the NPs in the membrane was analyzed. As shown in **Figure 3a–b**, the surface morphology of the PDA/PEI-NP 2 membrane (the mass of filtrated NP is 240 μg) did not change significantly after two hours of operation in pure water. Over time, the NPs on the membrane surface exhibited deformed and irregular shapes, whereas the NPs inside the membrane remained intact after continuous operation for 120 h (Figure 3c). Subsequently, the operating pressure was increased to 1.0 bar, and the membranes operated continuously for ten days. The membrane surface was smooth, although intact NPs were observed in certain pores (Figure 3d). The cross-sectional morphologies of the membranes were investigated through scanning electron microscopy (SEM) after 10 d of operation at 1.0 bar. As shown in Figure 3e-f, intact NPs were observed on the smooth surface of the membrane, and the NPs inside the membrane remained intact.

These results indicated that the NPs stably adhered to the pores inside the membrane. The surface morphology of the membrane was affected by pressure and time. In contrast, the NPs inside the membrane remained intact because they selectively accumulated at the dead end of the pores, and the covalent bonds inside the NPs inhibited polymer leaching caused by fluid erosion, which reflected the high long-term stability of the proposed membrane

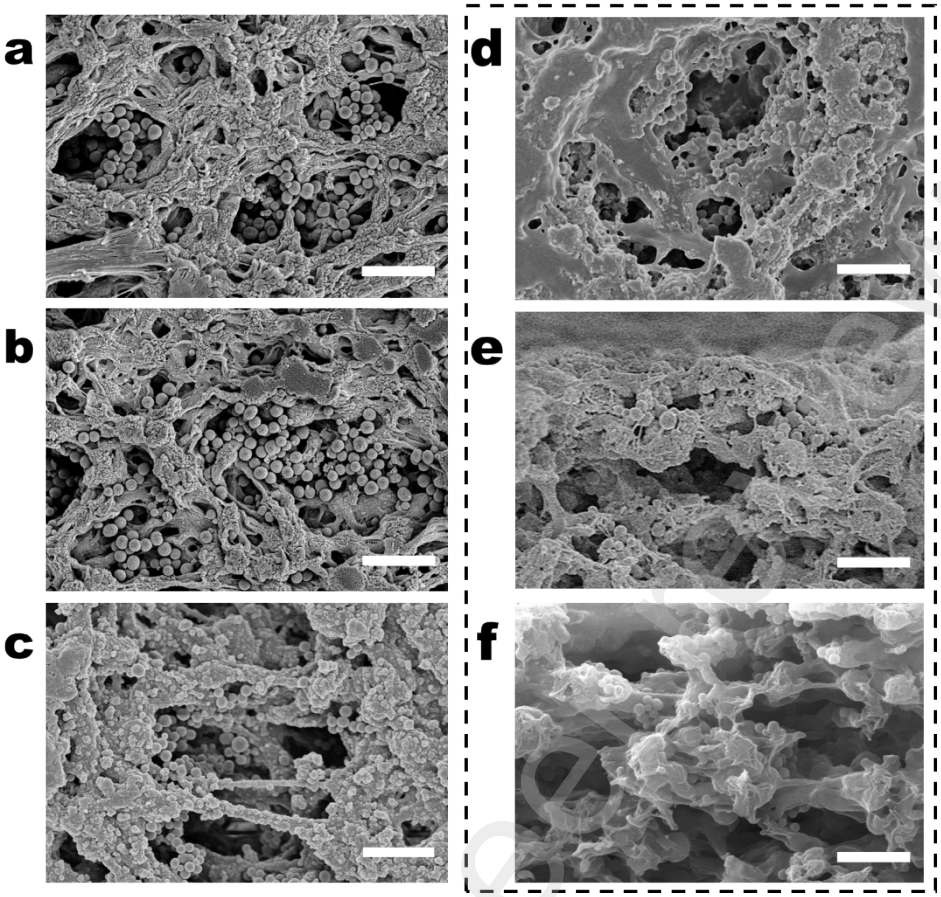

200

201 **Figure 3.** Stability of NPs in membranes. SEM images of (a) PDA/PEI-NP 2 membrane
202 surface; (b) PDA/PEI-NP 2 membrane surface after 2 h operation in pure water at 0.1 bar; (c)
203 PDA/PEI-NP 2 membrane surface after 120 h operation in pure water at 0.1 bar. SEM images
204 of (d) PDA/PEI-NP 2 membrane surface and (e–f) cross-section after 10 d operation in pure
205 water at 1.0 bar.

206

2.4 Wettability of NP membranes

As shown in **Figure 4a–d**, the hydrophilicity of the membrane surface was positively related to the NP loading. The original surface contact angle of the co-deposited membrane was 44.6 ±2.7°. As the NP loading increased, the contact angles of the PDA/PEI-NP 1–3 membranes were 40.9±1.8 °, 34.3±2.1°, and 24.1±3.3°, respectively. Furthermore, the droplet infiltration time was significantly different for different membranes. As shown in **Figure S1**, 0.1 mL water droplets were simultaneously dropped onto the co-deposited membrane and PDA/PEI-NP 2 membrane. After 71 s, water droplets could be observed on the co-deposited membrane but not on the PDA/PEI-NP 2 membrane. The dynamic contact angle indicated that the time for 5 μL droplets to penetrate the co-deposited membrane and PDA/PEI-NP 1–3 membranes was 4.33±0.12 s, 3.21±0.15 s, 2.39±0.14 s, and 3.58±0.25 s, respectively. These results indicated that the droplet infiltration time in the membrane decreased and then increased with increasing NP loading. The droplet infiltration time of the PDA/PEI-NP 2 membrane was the lowest.

Figure S2 demonstrates the underwater oil adhesion performance of the membranes. Oil droplets were attached to the PVDF and PDA/PEI-NP 2 membranes under water. The oil droplets adhered to the PVDF membrane, whereas oil droplets slipped away from the PDA/PEI-NP 2 membrane with no adhesion. According to the contact angle measurements (Figure 4 e–f), no significant adhesion was observed when the oil-droplet-contacted PDA/PEI-NP 2 membranes were extruded and removed. Additionally, the underwater oil contact angles of *n*-heptane and dichloromethane were 177.1±2.4° and 169.5±1.7°, respectively.

These results indicated that the hydrophilicity of the NP-supported membranes was enhanced with the increase in the number of oxygen-containing and amino groups on the membrane surface. Nevertheless, the increased hydrophilicity did not necessarily decrease the time required for the water droplets to penetrate the membrane. In general, the infiltration time of water droplets reflects the ability of water to penetrate the membrane pores. A small infiltration time indicates that a strong Laplace pressure or low resistance is generated when water enters the membrane, which decreases the threshold pressure during membrane separation and increases the membrane flux. This correlation can be expressed as follows [20]:

$$\Delta P = \Delta P_1 + \Delta P_2 = \frac{\pi C \mu}{\varepsilon r} J_V + \frac{7.94 \times 10^9 L}{\varepsilon r \theta} J_V \quad (1)$$

where ΔP is the total pressure drop, ΔP_1 is the pressure drop at the pore entrance/exit, ΔP_2 is the pressure drop inside the nanopore, C is the loss coefficient of both the water entry and exit processes, μ is the liquid viscosity, ε is the porosity, θ is the contact angle, and r is the maximum pore size. Notably, the membrane permeability is related to the intrinsic properties of the geometric and chemical structures of the membrane.

In this study, the PDA/PEI-NP 3 membrane exhibited the highest hydrophilicity. However, the median pore size of this membrane (600.20 nm) was lower than those of the co-deposited and PDA/PEI-NP 2 (668.75 nm and 653.92 nm, respectively), which hindered the droplet penetration (**Figure S5c–d**). In comparison, the PDA/PEI-NP 2 membrane exhibited a moderate hydrophilicity and pore size, which facilitated droplet infiltration. These findings highlighted that both the hydrophilicity and pore size of the membrane must be modified to decrease the droplet penetration time and increase the membrane flux.

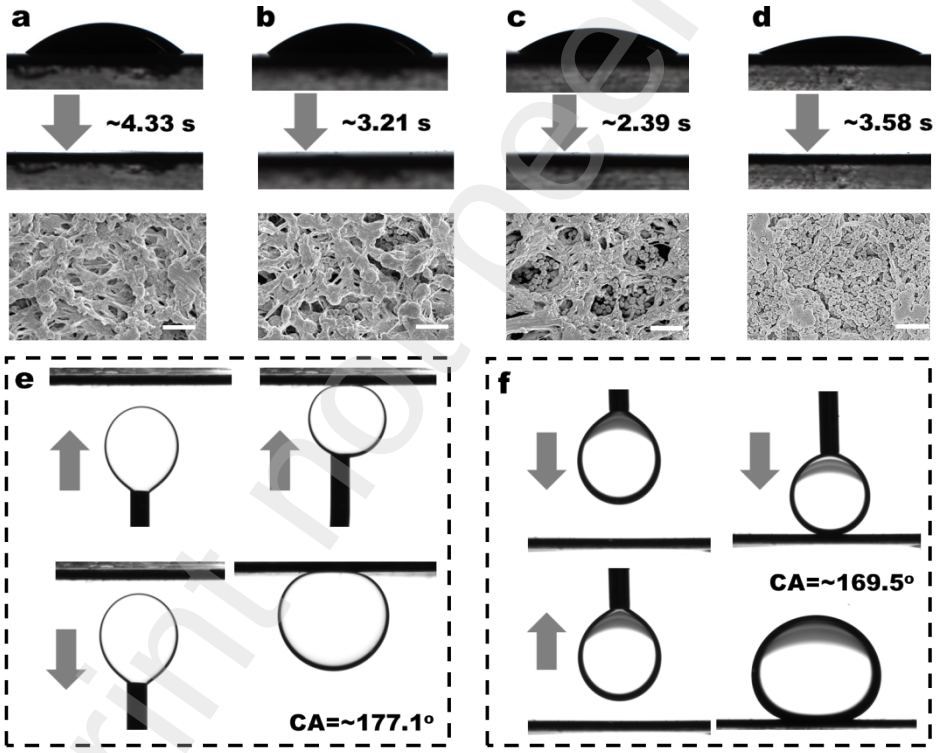

Figure 4. Surface wettability of NP membranes. Water contact angles (top) and surface morphologies (SEM, bottom, scale bars are 2 μm) of the (a) co-deposited membrane and PDA/PEI-NP (b) 1, (c) 2, and (d) 3 membranes. Underwater oil adhesion performance of (e) *n*-heptane and (f) dichloromethane.

2.5 Separation and antifouling performance of the NP membranes

To quantify the separation and antifouling performance of the membranes, the pure water flux, rejection rate, and flux recovery of the membranes in an oil-in-water emulsion were tested under crossflow conditions (**Figure 5**). First, the pure water fluxes of the co-deposited, PDA/PEI-NP 1–3 membranes were tested at 0.1, 0.3, 0.5, 0.8, and 1.0 bar. The pure water permeability coefficients (slopes) of the membranes were obtained through the linear fitting of the corresponding fluxes under different pressures. This procedure was repeated thrice to obtain the average value. As shown in Figure 5a, the pure water permeability coefficients of the co-deposited and PDA/PEI-NP 1–3 membranes were 9547.81±51.25, 10015.73±84, 10647.29±49, and 9237.88±45 $L \cdot m^{-2} \cdot h^{-1} \cdot bar^{-1}$, respectively, indicating that the membrane flux increased and then decreased with increase in the NP loading. The PDA/PEI-NP 2 membrane exhibited the highest flux.

The antifouling performance of the PDA/PEI-NP 2 membrane is shown in Figure 5b. The initial pure water flux at 0.1 bar was 1056.01 $L \cdot m^{-2} \cdot h^{-1}$. During the separation of the *n*-heptane–water emulsion, the membrane flux decreased to 317–500 $L \cdot m^{-2} \cdot h^{-1}$, although the pure water flux returned to its initial level after rinsing with pure water. After five cycles, the final pure-water flux of the membrane was 1001.54 $L \cdot m^{-2} \cdot h^{-1}$. The total flux decay and recovery rates were 5.16% and 94.84%, respectively. Similar experimental results were obtained for the separation of the dichloromethane–water emulsion (the total flux recovery rate was 92.95%, **Figure S3d**).

Moreover, the *n*-heptane–water emulsion was separated using the PDA/PEI-NP 2 membrane at 0.1 bar (Figure 5c). The appearance of the oil-in-water emulsion changed from white to transparent after the membrane separation. According to the characterization based on optical microscopy (**Figure S4**), the oil droplets were densely distributed in the oil-in-water emulsion, whereas no emulsion oil droplets were found on the permeate side after membrane separation. Moreover, the rejection rates of the membrane into the *n*-heptane-in-water emulsion, dichloromethane-in-water emulsion, and peanut oil-in-water emulsion were 99.20±0.16%, 99.47±0.16%, and 99.17±0.13%, respectively, higher than that of the co-deposited membrane (Figure 5d).

These results highlighted that the pure water fluxes of the PDA/PEI-NP 1 and 2 membranes were superior to those of the co-deposited membranes. This phenomenon occurred because the

NPs did not block the flow-through pores and enhanced the hydrophilicity of the membrane, resulting in a decreased threshold pressure. The pure water permeation flux of the PDA/PEI-NP 3 membrane was lower than that of the co-deposited membrane, likely because the membrane pores were narrowed owing to the presence of excessively many NPs and high fluid transfer resistance across the membrane. Furthermore, the pure water flux of the PDA/PEI-NP 2 membrane was higher than those reported in previous studies (Table S1). In addition, the PDA/PEI-NP 2 membrane exhibited high rejection and antifouling performances for *n*-heptane– and dichloromethane–water emulsions.

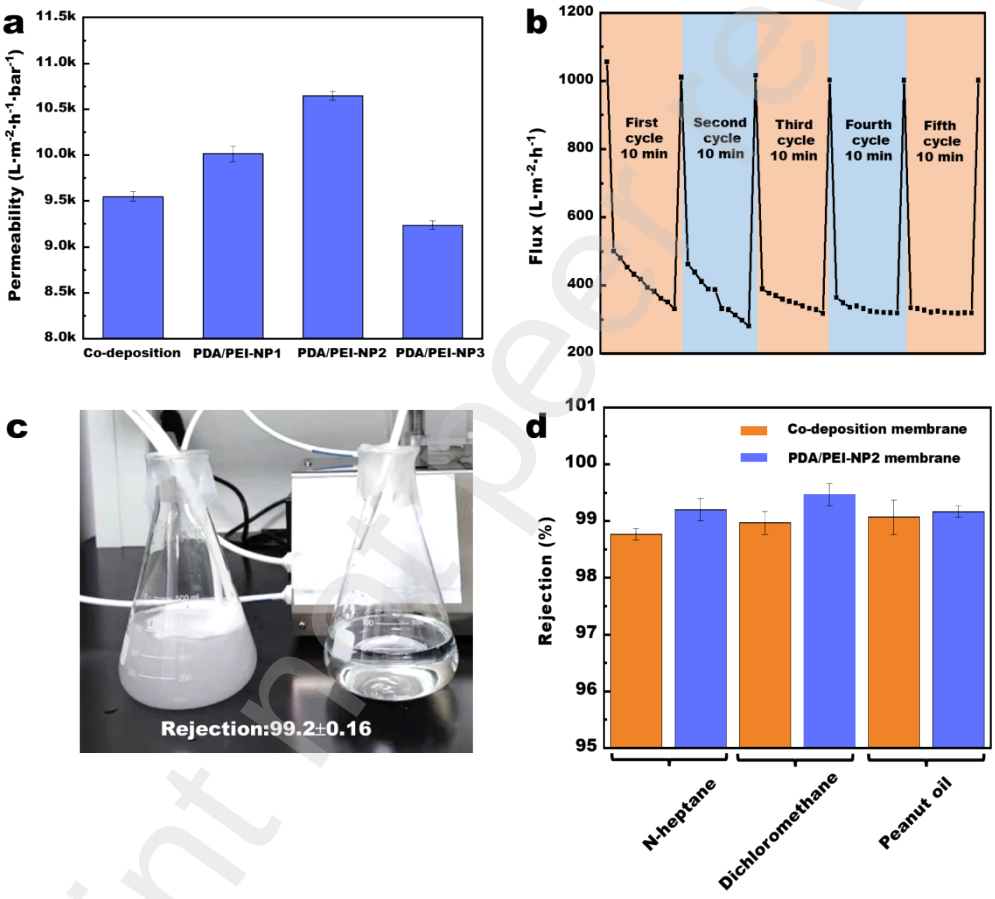

Figure 5. Separation and antifouling performance of membranes under crossflow conditions. (a) Permeability coefficients of the co-deposited and PDA/PEI-NP 1–3 membranes (temperature = 25±2 °C); (b) flux recovery of the PDA/PEI-NP 2 membrane after five cycles (membrane separation of *n*-heptane–water emulsion and rinsing with pure water). (c) Photographs of the separation of the *n*-heptane–water emulsion; (d) different oil-in-water rejection rates for the co-deposited and PDA/PEI-NP 2 membranes.

2.6 Stability of NP membranes

Figure 6 shows the stability values of the PDA/PEI-NP 2 membrane. First, flux changes of the PDA/PEI-NP 2 and co-deposited membranes that operated in pure water for 2 h at 0.1 bar were compared (Figure 6a). The flux of the PDA/PEI-NP 2 membrane was nearly stable (ranging between 1050 and 1080 $L \cdot m^{-2} \cdot h^{-1}$), whereas that of the co-deposited membrane increased from 956.2±12.67 to 1051.8±17.33 $L \cdot m^{-2} \cdot h^{-1}$ in 40–60 min. The antifouling and separation performances of the co-deposited membrane also varied (Figure 6b–c). As shown in Figure 6b, the flux decay of the co-deposited membrane increased within three cycles at 0.1 bar, and the total flux decay rate was 17.52%. However, the pure water flux of the membrane increased to 1063.27 $L \cdot m^{-2} \cdot h^{-1}$ at the beginning of the fourth cycle, and this value was higher than the initial flux of the co-deposited membrane (951.71 $L \cdot m^{-2} \cdot h^{-1}$). The membrane flux decay increased again in the fourth and fifth cycles. The total flux decay rate of co-deposited membrane after five cycles was –1.97%. In addition, the rejection rate of the co-deposited membrane for the *n*-heptane-in-water emulsion in each cycle was measured (Figure 6c). The rejection rate decreased from 99.51±0.16% in the third cycle to 97.86±0.13% in the fourth cycle, consistent with the moment of flux increase at the beginning of the fourth cycle. Nevertheless, the rejection rate and antifouling performance of the PDA/PEI-NP 2 membrane did not change significantly over the five cycles. Similar phenomena were observed in the rejection and antifouling experiments with dichloromethane and peanut oil (Figure S3). Finally, the long-term stabilities of the PDA/PEI-NP 2 membranes were investigated (Figure 6d). It was noted that the membrane flux remained stable (decreased from 1083 $L \cdot m^{-2} \cdot h^{1}$ to 1036 $L \cdot m^{-2} \cdot h^{-1}$) for 120 h at 0.1 bar.

These results indicated that the long-term stability and separation performance of the PDA/PEI-NP 2 membrane were superior to those of the co-deposited blank membrane. The limited long-term stability of the co-deposited membrane could be attributed to the unstable co-deposited coating, which readily underwent leaching under the experiment conditions. As shown in Figure S5a–b, after 2 h of consecutive operation, the median pore size of the co-deposited membrane increased from 668.75 to 686.55 nm, and the porosity increased from 65.63% to 67.76%. This phenomenon likely occurred because the fluid flow rate on the membrane surface was high (1.3 $m \cdot s^{-1}$) under crossflow conditions, and the surface coating underwent leaching. Inside the membrane, the friction between the fluid and pore walls likely led to the leaching of the polymers because of the reversible coordination bonds between the co-deposition layer and PVDF. Because the coating inside the membrane was a uniformly distributed polymer with a

small molecular size, the polymer did not block the pores after leaching, resulting in large pores, which increased the membrane flux and decreased the rejection rate. Nevertheless, as shown in Figure S5e–f, after successive operation for 120 h, the median pore size of the PDA/PEI-NP 2 membrane decreased from 653.92 to 651.11 nm, and the porosity increased from 64.73% to 64.97%, which pertain to negligible changes. In the case of the PDA/PEI-NP 2 membrane, most of the NPs were supported inside the membrane. Compared with the high-speed fluid on the surface, the fluids inside the membrane exhibited creeping flow (for a membrane flux of 1064.73 $L \cdot m^{-2} \cdot h^{-1}$, the water flow rate inside the membrane was 0.0000296 $m \cdot s^{-1}$) and thus could not leach the large NPs that adhered to the dead ends. Moreover, covalent bonds were formed in the NPs through Michael addition or the Schiff base reaction, which inhibited the leaching of polymers on the NP surface caused by creeping. Consequently, the proposed membrane exhibited high long-term stability.

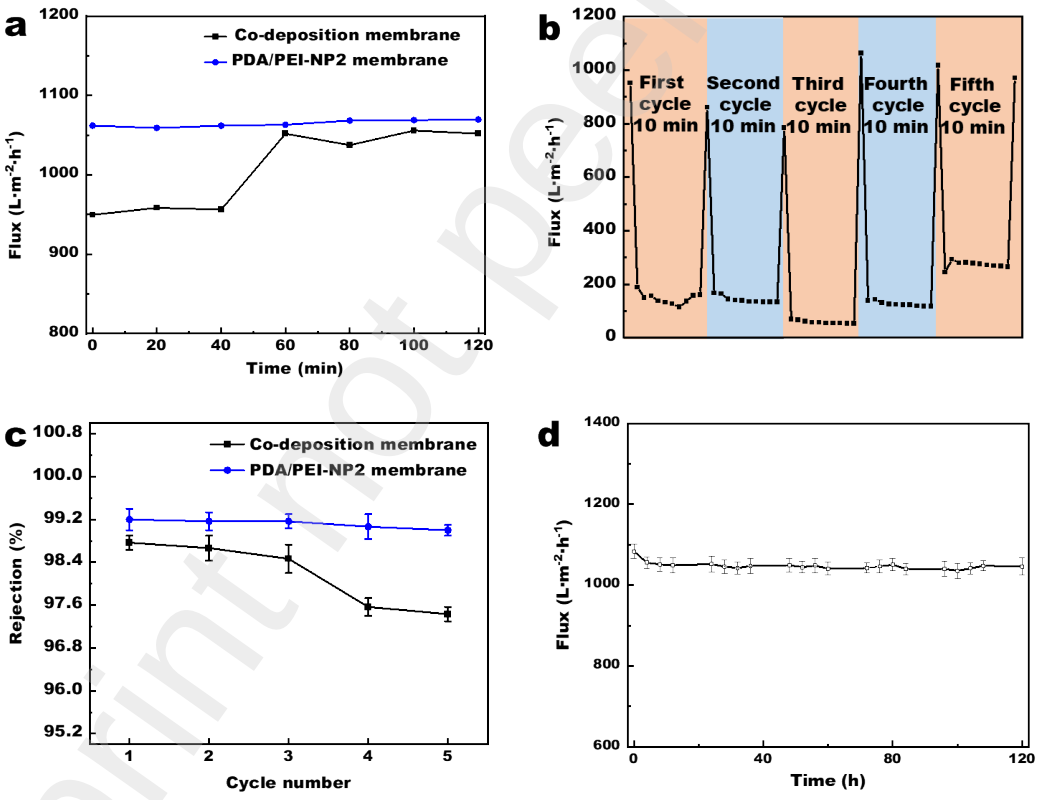

Figure 6. Stability of the PDA/PEI-NP 2 membrane under crossflow with an operating pressure of 0.1 bar. (a) Flux of the co-deposited and PDA/PEI-NP 2 membranes in pure water operation for 2 h (temperature = 25±2 °C). (b) Flux recovery of the co-deposited membrane over five cycles of membrane separation of *n*-heptane–water emulsion and rinsing with pure water. (c) Rejection rates of the co-deposited and PDA/PEI-NP 2 membranes in five cycles. (d) Flux of the PDA/PEI-NP 2 membrane during successive operation for 120 h at 0.1 bar.

3. Conclusions

PDA/PEI-NP membranes were prepared by supporting PDA/PEI NPs in the interior of co-deposited PVDF membranes through self-assembly. The flow rate inside the membrane was considerably smaller than the high-speed water flow rate under crossflow conditions. Consequently, large NPs, which exhibited the formation of covalent bonds and adhered to the dead end of the pores inside the membrane, were not easily leached. Therefore, the PDA/PEI-NP membranes exhibited higher long-term stability. Additionally, because the NPs did not block the flow-through pores, thereby increasing the hydrophilicity of the membrane, the flux of the PDA/PEI-NP membrane increased, and its antifouling ability was enhanced compared with that of the co-deposited membrane. This study sets the first example of selectively supporting nanoparticle inside polymer membrane to fabricate a membrane with long-term stability and excellent separation performance by a facile method. We anticipate that the findings in this study can enlighten the sustainable development of membrane technology.

4. Experimental

*Materials***.** The PVDF membrane (average pore size = 0.45 μm, Cytiva, USA), PES membrane (average pore size = 0.45 μm, Shanghai Dibo Biotechnology, China), and MCE membrane (average pore size = 0.45 μm, Beyotime Biotechnology, China) were purchased. Dopamine hydrochloride and polyethyleneimine (molecular weight = 600 Da) were purchased from Shanghai Aladdin Biochemical Technology Co. Ltd., China. NaOH, Tween-80, *n*-heptane, dichloromethane, and ethanol were purchased from Shanghai Macklin Biochemical Technology Co. Ltd., China. All chemical reagents were used directly without further purification. The peanut oil was purchased from a local supermarket.

*Synthesis of PDA NPs***.** Dopamine hydrochloride (0.506 g) was dissolved in deionized water (300 mL). NaOH (1.7 mL, 1 $mol \cdot L^{-1}$) was added, and the solution was shaken at 50 ℃ for 6 h. After the reaction was complete, the NPs were subjected to high-speed centrifugation (6000 rpm, 20 min) and rinsed repeatedly with deionized water. Subsequently, the NPs were dispersed in deionized water by ultrasonication to obtain a PDA NP dispersion.

*Synthesis of PDA/PEI NPs***.** Dopamine hydrochloride (0.506 g) was dissolved in deionized water (300 mL). NaOH (1.7 mL, 1 $mol \cdot L^{-1}$) was added, and the solution was shaken at 50 ℃ for 3.5 h. Subsequently, PEI (0.253 g) was added to this solution and shaken at 35 ℃ for 2 h.

After the reaction was complete, the NPs were subjected to high-speed centrifugation (6000 rpm, 20 min) and rinsed repeatedly with deionized water. Later, these NPs were dispersed in deionized water through ultrasonication to obtain a PDA/PEI-NP dispersion.

*Fabrication of the co-deposited PVDF membrane***.** A round PVDF membrane (diameter of 17 cm) was cut and placed in a Buchner funnel, followed by the addition of ethanol (50 mL, to completely wet the membrane) and vacuum filtration. Subsequently, deionized water (200 mL) was added, and vacuum filtration was continued. Later, the membrane was stored in deionized water. Dopamine hydrochloride (0.506 g) and PEI (0.506 g) were dissolved in NaOH solution (300 mL; 1.7 mL, 1 $mol \cdot L^{-1}$). The PVDF membrane was immersed in the prepared solution, which was placed in a water bath isothermal oscillator and shocked at 50 ℃ for 10 h. Upon completion of the reaction, the PVDF membrane was thoroughly rinsed with deionized water to obtain a PDA/PEI co-deposited modified PVDF membrane.

*Fabrication of the PDA/PEI-NP membranes***.** A round co-deposited membrane (diameter of 7.5 cm) was cut and placed in a filtration device with a filtration diameter of 6 cm, and the mixed solution (2 L) was added to the filtration cup for vacuum filtration (vacuum pressure = 0.8 bar). After thermal treatment at 50 ℃ for 10 h, the membranes were thoroughly rinsed with deionized water. Membranes with NP concentrations of 60, 120, and 300 μg/L were labeled PDA/PEI-NP 1, 2, and 3, respectively.

*Characterization***.** The PDA/PEI NPs and PDA/PEI-NP membranes were characterized by FESEM (Hitachi, SU8020, Japan and Oxford, TESCAN MIRA4) to observe the surface and cross-sectional morphologies. The cross-sectional morphologies were obtained by wetting the membrane with liquid nitrogen and sputtering the samples with gold before analysis. The elemental composition and functional groups of the materials were determined by XPS (Thermo Fisher, 250Xi), implemented using an X-ray source and Al target (Kα ray, 1486.60 eV). The KBr pellet method and ATR mode of an FTIR instrument (iS10) were employed to analyze the functional groups of the powder and membrane samples, respectively, under the following conditions: wavenumber range = 400–4000 cm^{-1}, resolution = 4 cm^{-1}, signal-to-noise ratio = 50000:1, and number of scans = 64. The size distribution of the NPs was analyzed using a laser particle size analyzer (Zetasizer Nano ZS90). A contact angle goniometer (DataPhysics, OCA 50) was used to determine the dynamic contact angle of the membrane in air, adhesion capability of the membrane to different oils, and underwater static contact angle of the

membrane. Measurements for each sample were obtained five times, and the average value was determined (the droplet volume was 5 μL). The pore sizes and porosities of the membranes were measured using a high-performance automatic mercury injection instrument (Micromeritics Instrument Corporation, AutoPore LV 9510). The oil concentration in the oil-in-water emulsion was measured using an ultraviolet-visible spectrophotometer (UV2600; Shimadzu, Japan).

*Evaluation of membrane separation and antifouling properties***.** The separation and antifouling performances of the membranes were evaluated using a crossflow membrane filtration device (MFT, Guochu Technology, China). Before testing, all the membranes were operated in deionized water at 1.0 bar for 15 min to ensure system stability. The permeability in pure water was tested for 10 min at 0.1, 0.3, 0.5, 0.8, and 1.0 bar. Measurements for each sample were obtained three times, and the average value was considered the result. The pure water flux of the proposed membrane was calculated as follows:

$$J_V = \frac{V}{A\Delta t} \tag{2}$$

where J_v is the pure water flux of the membrane ($L \cdot m^{-2} \cdot h^{-1}$), V is the permeable volume (L) of pure water per unit time (Δt), and A is the separation area (m^2) of the membrane.

An oil-in-water emulsion was prepared before the antifouling test. Specifically, *n*-heptane (0.9 g) and Tween-80 (0.1 g) were added to water (1.0 g), and the solution was stirred at 4000 rpm for 24 h to obtain an oil-in-water emulsion. Moreover, oil-in-water emulsions with dichloromethane and peanut oil were prepared using the same procedure. When evaluating the antifouling and separation performances of the membrane samples, the stable flux of the oil-in-water emulsion was denoted as J_o, and the overall flux decay rate was calculated from J_v and J_o:

$$DR = \left(1 - \frac{J_o}{J_v}\right) \times 100\% \tag{3}$$

where DR is the total flux decay rate of the membrane.

The rejection rate of the oil-in-water emulsion by the membrane was determined as

$$R = \left(1 - \frac{C_0}{C_1}\right) \times 100\% \tag{4}$$

where R is the membrane rejection rate, C_1 is the oil concentration on the feed side ($mg \cdot L^{-1}$), and C_0 is the oil concentration on the permeate side ($mg \cdot L^{-1}$). The oil concentrations were quantified by measuring the UV absorbance at 530 nm.

*Membrane stability***.** The long-term stability of the proposed membranes was evaluated by monitoring the pure water flux at 0.1 bar for five consecutive days. Samples were collected every 4 h from 9:00 to 21:00 to measure the membrane flux. The deionized water was replaced after each measurement. After the experiment, the membrane was extracted and characterized using SEM (before and after long-term operation) to observe the NPs on the membrane surface and inside the membrane. The operating pressure was increased to 1.0 bar for ten consecutive days. After the experiment, the membrane was removed and characterized using SEM (before and after long-term operation) to observe the NPs on the membrane surface and inside the membrane.

Acknowledgments

M. Long is acknowledged for assisting with the Scanning Electron Microscopy (SEM) characterization of nanoparticles inside membrane (Figure 3f). Weily editing services is acknowledged for providing language help, writing assistance and proof reading of the article.

Funding

Financial support with a grant number of 42177065 is acknowledged by the authors to the National Natural Science Foundation of China; Financial support with a grant number of 2021M700889 is acknowledged by the authors to the China Postdoctoral Science Foundation; Financial support with grant numbers of 2020B1111530001 and 2019QN01L682 are acknowledged by the authors to the Guangdong Foundation for Program of Science and Technology Research; Financial support with grant numbers of 2020GDASYL-20200102013 and 2020GDASYL-20200101002 are acknowledged by the authors to the GDAS Special Project of Science and Technology Development; Financial support with grant numbers of CRRP2020-03MY-He is acknowledged by the authors to the Asia-Pacific Network for Global Change Research" APN project.

References

[1] M.A. Shannon, P. W. Bohn, M. Elimelech, J. G. Georgiadis, B. J. Marinas, A. Mayes, Science and technology for water purification in the coming decades, Nature 452 (2008) 301−310.

[2] D. S. Sholl, R. P. Lively, Seven chemical separations to change the world, Nature 532 (2016) 435–437.

[3] B. D. Park, J. Kamcev, L. M. Robeson, M. Elimelech, B. D. Freeman, Maximizing the right stuff: The trade-off between membrane permeability and selectivity, Science 356 (2017) 1138–1148.

[4] S. Zhang, G. Jiang, S. Gao, H. Jin, Y. Zhu, F. Zhang, J. Jin, Cupric Phosphate Nanosheets-Wrapped Inorganic Membranes with Superhydrophilic and Outstanding Anticrude Oil-Fouling Property for Oil/Water Separation, ACS Nano 12 (2018) 795–803.

[5] D. L. Gin, R. D. Nobel, Chemistry. Designing the next generation of chemical separation membranes, Science 332 (2011) 674–676.

[6] D. J. Miller, D. R. Dreyer, C. W. Bielawski, D. R. Paul, B. Freeman, Surface Modification of Water Purification Membranes, Angew. Chem. Int. Ed. 56 (2017) 4662–4711.

[7] S. Y. Wang, L. F. Fang, R. Takagi, H. Matsuyama, Development of membranes with well-dispersed polyampholytic copolymer via a composite coagulation process, J. Membr. Sci. 620 (2021) 118848.

[8] Y. Wen, J. Yuan, X. Ma, S. Wang, Y. Liu, Polymeric nanocomposite membranes for water treatment: a review, Environ. Chem. Lett. 17 (2019) 1539–1551.

[9] H. C. Yang, R. Z. Waldman, M. B. Wu, J. Hou, L. Chen, S. B. Darling, Z. K. Xu, Dopamine: Just the right medicine for membranes, Adv. Funct. Mater. 28 (2018) 1705327.

[10] H. Lee, S. M. Dellatore, W. M. Miller, P. B. Messersmith, Mussel-Inspired Surface Chemistry for Multifunctional Coatings, Science 318 (2007) 426–430.

[11] D. Guo, Y. Xiao, T. Li, Q. Zhou, L. Shen, R. Li, Y. Xu, H. Lin, Fabrication of high-performance composite nanofiltration membranes for dye wastewater treatment: mussel-inspired layer-by-layer self-assembly, J. Colloid Interf. Sci. 560 (2020) 273–283.

[12] Y. Zhang, J. Guo, G. Han, Y. Bai, Q. Ge, J. Ma, C. H. Lau, L. Shao, Molecularly soldered covalent organic frameworks for ultrafast precision sieving, Sci. Adv. 7 (2021) abe8706.

[13] R. Liu, Q. Chen, M. Cao, J. Lin, F. Lin, W. Ye, P. Lius, B. V. Bruggen, S. Zhao, Robust bio-inspired superhydrophilic and underwater superoleophobic membranes for simultaneously fast water and oil recovery, J. Membr. Sci. 623 (2021) 119041.

[14] S. Yang, L. Y. Zou, C. Liu, Q. Zhong, Z. Y. Ma, J. Yang, J. Ji, P. Müller-Buschbaum, Z. Xu, Codeposition of Levodopa and Polyethyleneimine: Reaction Mechanism and Coating Construction, ACS Appl. Mater. Interfaces 12 (2020) 54094–54103.

[15] H. C. Yang, K. J. Liao, H. Huang, Q. Y. Wu, L. S. Wan, Z. K. Xu, Mussel-inspired modification of a polymer membrane for ultra-high water permeability and oil-in-water emulsion separation, J. Mater. Chem. A 2 (2014) 10225–10230.

[16] M. Long, Y. Ma, C. Yang, R. Zhang, Z. Jiang, Superwetting membranes: from controllable constructions to efficient separations, J. Mater. Chem. A 9 (2021) 1395–1417.

[17] J. Hu, X. D. Xiao, D. F. Ogletree, M. Salmeron, Imaging the Condensation and Evaporation of Molecularly Thin Films of Water with Nanometer Resolution, Science 268 (1995) 267–269.

[18] S. Chen, F. Yu, Q. Yu, Y. He, S. Jiang, Strong Resistance of a Thin Crystalline Layer of Balanced Charged Groups to Protein Adsorption, Langmuir 22 (2006) 8186–8191.

[19] J. R. Werber, C. O. Osuji, Materials for next-generation desalination and water purification membranes, Nat. Rev. Mater. 1 (2016) 16018.

[20] X. Fang, M. J. Wei, X. Zhang, Y. Wang, Effect of hydrophilicity on water transport through sub-nanometer pores, J. Membr. Sci. 611 (2020) 118297.

[21] F. Xu, M. Wei, C. Zhang, Y. Song, W. Zhou, Y. Wang How Pore Hydrophilicity Influences Water Permeability? Research, 001 (2019) 66–76.

[22] H. Sun, Y. Du, C. Gao, J. Long, S. Li, L. Shao, Pressure-assisted in-depth hydrophilic tailoring of porous membranes achieving high water permeability, excellent fouling resistance and superior antimicrobial ability, J. Membr. Sci. 604 (2020) 118071.

[23] H. Lee, N. F. Scherer, P. B. Messersmith, Single-molecule mechanics of mussel adhesion, Proc. Natl. Acad. Sci. 103 (2006) 12999–13003.

[24] W. Cheng, X. Zeng, H. Z. Chen, Z. M. Li, W. F. Zeng, L. Mei, Y. L. Zhao, Versatile Polydopamine Platforms: Synthesis and Promising Applications for Surface Modification and Advanced Nanomedicine, ACS Nano 13 (2019) 8537–8565.

Graphical abstract